npj | science of food

Article

Published in partnership with Beijing Technology and Business University

https://doi.org/10.1038/s41538-024-00344-0

Perforated imprinting on high moisture meat analogue confers long range mechanical anisotropy resembling meat cuts

Xuanming Lou[1], Jiahao Wang[2], Leng Gek Kwang[2], Hanzhang Zhou[1,3,4], Francesca Yi Teng Ong[5], Shengyong Ng[6] & Hanry Yu[1,2,3,4,5,6,7,8]

Meat cuts, when cooked and masticated, separate into fibrous structures because of the long-range mechanical anisotropy (LMA) exhibited by muscle fascicles, which is not fully recapitulated in alternative proteins produced using molecular alignment technology like high moisture extrusion. We have developed a scalable perforated micro-imprinting technology to greatly enhance LMA in high moisture meat analogue (HMMA). By imprinting 1 mm thick HMMA sheets with perforated patterns (optimized by AI), we observed up to 5 × more anisotropic separation of fibrous structures in a one-dimensional pulling LMA analysis, to match the fibrousness of the cooked chicken breast, duck breast, pork loin and beef loin. We stacked and bound imprinted sheets with transglutaminase (TG) to produce imprinted whole-cuts. Controlling fiber separation in the imprinted cuts achieved hardness ranging from 6578 g to 18467 g (2 cm × 2 cm × 1 cm, 50% strain), which matched meats from different species. Imprinted cuts improved meat-like fiber separation over HMMA when masticated, measured by Euclidean distances (0.057 and 0.106 respectively) to animal meat cuts on image features. In sensory evaluation, imprinted cuts improved consumer acceptance by 33.3% and meat-like fibrousness by 20%, by significantly enhancing the HMMA appearance, texture, and mouthfeel.

The increasing global population intensifies environmental pressures associated with traditional livestock-based meat production[1,2]. Plant-based meat (PBM), derived from texturized plant proteins, has emerged as a sustainable alternative[3,4]. PBM has progressed with decreasing cost[5,6] and improved flavor over the past decades[7]. One of the major bottlenecks has been the lack of the PBM version of whole-cut meat with appearance and texture of chicken breast, beef steak, etc[8]. The appearance and mouthfeel of whole-cut meat are mainly determined by the tightly packed and aligned meat fibers which separate upon cooking and mastication, i.e. the fibrousness of whole meat cut[9].

Fibrousness of meat cut correlates with mechanical anisotropy, which refers to the variation of mechanical properties depending on the direction of mechanical load. In fibrous meat cuts, longitudinal loads tearing the fibers are carried by the strength of the fibers, while transverse loads separating the fibers depend on their bonding[10]. Cooking partially breaks the bonding between fibers[11,12], causing them to separate transversely under mechanical loads like compression or biting, instead of tearing longitudinally[13,14]. This transverse separation during consumption generates long, thick fibers (>millimeter) in meat cuts that differs from the microfibrils of minced meat[15,16], which is crucial for the fibrous appearance and mouthfeel of meat cuts[14,17]. The mechanical anisotropy at the muscle fascicle scale may be critical for fiber separation in meat cuts, as cooking more significantly breaks the intra-fascicle bonding at this long-range (>millimeter) scale compared

[1]Department of Physiology, The Institute for Digital Medicine (WisDM), Yong Loo Lin School of Medicine, National University of Singapore, Singapore, 117593, Singapore. [2]Mechanobiology Institute, National University of Singapore, Singapore, 117411, Singapore. [3]Integrative Sciences and Engineering Programme (ISEP), NUS Graduate School, National University of Singapore, Singapore, 119077, Singapore. [4]Bioprocessing Technology Institute (BTI), A*STAR, 20 Biopolis Way, Singapore, 138668, Singapore. [5]Department of Biomedical Engineering, College of Design and Engineering, National University of Singapore, Singapore, 117583, Singapore. [6]Ants Innovate Pte. Ltd., #12-07 Suntec Tower One, Temasek Boulevard, Singapore, 038987, Singapore. [7]Critical Analytics for Manufacturing Personalized Medicine (CAMP), Singapore-MIT Alliance for Research and Technology, Singapore, 138602, Singapore. [8]Institute of Bioengineering & Bioimaging (IBB), A*STAR, Singapore, 138669, Singapore. e-mail: phsyuh@nus.edu.sg

to smaller intra-fascicle scales[13,18]. The long-range mechanical anisotropy (LMA) correlates with the millimeter-scale fiber separation in meat cuts, producing long fibers distinct from minced meat. To replicate the fibrousness of meat cuts in whole-cut PBM, it might be essential to recreate this LMA.

Whole-cut PBM processing such as high moisture extrusion creates anisotropy by denaturing, stretching, and aligning plant protein molecules[19,20]. The protein molecules change their short-range structure from granules to fibrils[21,22]. The structural change at short range contributes to the development of meat-like bulk mechanical properties in the resulting product[23], high moisture meat analogue (HMMA). Despite the optimization of HMMA's structure at short range, it is insufficient to produce meat-like long-range fibrousness. The long-range structure of HMMA is mainly determined by the flow state of plant proteins in the cooling die connected after extruder[21]. Plant protein in the cooling die flows steadily to form layered structure of HMMA[19,24]. The layers rip apart into strings during deformation and create fibrousness[25]. The fibrousness by arbitrary ripping has limited similarity to animal meat likely due to the insufficient LMA to guide the fiber separation during its consumption.

HMMA exhibits meat-like bulk mechanical properties but lacks sufficient fibrousness. We hypothesize that perforated micro-imprinting structure at the muscle fascicle scale on HMMA sheets would confer the necessary LMA to enhance meat-like fibrousness. In this paper, a quantitative measurement of LMA (LMA index) was first established, highlighting its crucial role in shaping the morphological and mechanical properties of animal meat cuts. Next, a method was developed to directly imprint perforated patterns at muscle fascicle scale on sliced HMMA sheets. By optimizing the imprinting patterns, we achieved control of LMA index replicating different meats at the scale comparable to their muscle fascicles. Imprinted sheets were stacked and bound by transglutaminase (TG) to produce imprinted meat cuts with precisely controlled LMA that significantly improved meat-like fibrousness and texture. To streamline the design process of imprinting patterns for various meats, a computer vision model named MLCNet (Meat LMA Carving Network) was developed. This model recognizes varying LMA and facilitates the rapid and autonomous design of diverse imprinting patterns. To demonstrate the scalability of the method, a semi-continuous roller-based imprinter was constructed. Using this approach, a flamed chicken breast analogue was produced with the stacked imprinted HMMA sheets (imprinted cuts), showing significantly improved sensory profiles and meat-like fibrousness compared to the original HMMA control.

Results

The fibrousness of animal meat cuts correlates with the LMA at muscle fascicle scale

Meat cuts separate into long and thick fibers during its consumption, which differs from the microfibrils in minced meat[15,16]. The separation of thick fibers is likely due to the breaking of connections between muscle fascicles during cooking[13,18]. To systematically verify fiber separation most likely occurs at inter-fascicle scale rather than inner fascicles, we imaged the cross section of boiled meat cuts (chicken breast, duck breast, pork loin) using SEM and identified significant wide gap between muscle fascicles at millimeter scale (Figs 1a, and S1a). This finding was verified by optical coherence tomography (OCT), a non-destructive method to image subsurface structures. Fascicles of approximately 1 mm were observed to have wide longitudinal gaps between them (Figs. 1b and S1b). When subjected to compression/biting, the gaps between fascicles result in inter-fascicle separation occurring more readily at millimeter scale than inner fascicles (Figs. 1c and S1c). Compression/biting squeezes meat cuts and generates forces longitudinal and transverse to the fascicles (Fig. 1c). Inter-fascicle separation occurs because of the mechanical anisotropy that the fascicles resist tearing by the longitudinal force, while the transverse force easily separates them (Fig. 1c). Inter-fascicle separation creates long fibers with millimeter-scale thickness as a characteristic of meat cuts. We define the mechanical anisotropy at millimeter scale leading to separation of these fibers in meat cuts as long-range mechanical anisotropy (LMA).

To demonstrate LMA's impact on morphological and mechanical properties of animal meats, we performed tensile tests to characterize tearing process of meats. Tensile samples of various sizes were isolated from boiled meat cuts. It was observed under a high-speed camera that thick samples (diameter > 1 mm) were more likely to tear fibrously by forming multiple tensile cracks at different positions and times (Figs. 1d and S1d). In comparison, thinner samples (diameter < 1 mm) broke with a single crack spreading continuously across the sample (Figs. 1d and S1d). Similar differences in tearing process were reflected in mechanical measurements by universal testing machine[26]. Thick tensile samples often (> 80%) exhibited multiple tearing peaks on the strain-stress curves, consistent with the development of multiple cracks. In contrast, the thin samples typically (60–80%) broke with a single peak (Fig. 1e, Fig. S1e). The thick samples exceeding the scale of muscle fascicles exhibited fibrousness because of their LMA. The LMA at fascicle scale caused the fascicles to separate and tear individually (Fig. 1d, samples > 1 mm). Thin samples below the size of muscle fascicles lacked LMA and tore at one position with a single crack, showing no fibrousness.

To measure LMA and describe meat fibrousness quantitatively, we established a one-dimensional pulling approach as LMA analysis. In the LMA analysis, meat cuts were sliced to sheets ~1 mm thickness, followed by pulling the sheets until tearing to analyze their torn edges. Samples with more readily separated fibers tore fibrously, forming uneven edges. Conversely, the samples with more tightly bound fibers showed smooth and less fibrous edges (Fig. 1f). We quantified edge unevenness as the LMA index to describe the LMA and fibrousness of the samples. LMA index was defined by the standard deviation of differences between average heights of groups of dots on the torn edge (Fig. 1f). Higher LMA index indicated larger standard deviation, meaning more frequently abrupt rising/falling on the edges, and thus the edges were more uneven and fibrous (details provided in Supplementary Information). Different tested meats showed varying fibrousness levels that were quantitatively measured by their LMA indices, ranging from pork loin with an average LMA index of 0.37 to beef loin with an average LMA index of 1.12 (Fig. 1g). The tearing process of meat under a high speed camera can be found in the Supplementary Video.

HMMA has insufficient LMA to fully replicate meat cut-like fibrousness

HMMA is a promising whole-cut PBM that exhibits fibrousness and meat-like bulk mechanical properties[23]. The fibrousness of HMMA comes from its layered structure ripping apart during deformation[25] (Fig. 2a). When subjected to compressive loads, HMMA shows meat-like mechanical properties measured by texture profile analysis (TPA) (Figs. 2b and S2). To evaluate whether the fibrousness from HMMA's layered structure is close to animal meat cuts, we measured the LMA index of sliced HMMA sheets, showing an average value of 0.20, which was significantly lower than that of animal meats ($p < 0.05$) (Fig. 2c). Since HMMA's layered structure exhibits low LMA, it tore with smooth edges rather than fibrous uneven edges. This tearing behavior was further confirmed morphologically under a high-speed camera and mechanically by universal testing machine. Thick HMMA tensile samples (> 1 mm) tore by detaching between layers, instead of meat-like tearing of fibers (Fig. 2d), consistent with a lack of LMA in the layers. In mechanical measurements, thick HMMA tensile samples (> 1 mm) tore with a single breaking peak on the stress-strain curve, similar to the thin meat samples without LMA but different from meat samples of comparable size that showed multiple breaking peaks (Fig. 2e).

Due to the lack of LMA, the structural breakdown differences between HMMA and animal meats were observed not only in sliced sheets or tensile samples but also in the thick cuts of HMMA and boiled animal meats. Under compression, HMMA cuts with insufficient LMA deformed isotropically without direction preference, whereas animal meat cuts expanded anisotropically transverse to the fascicles and separated them at millimeter scale (Fig. 2f). We quantified breaking anisotropy using the aspect ratio of an

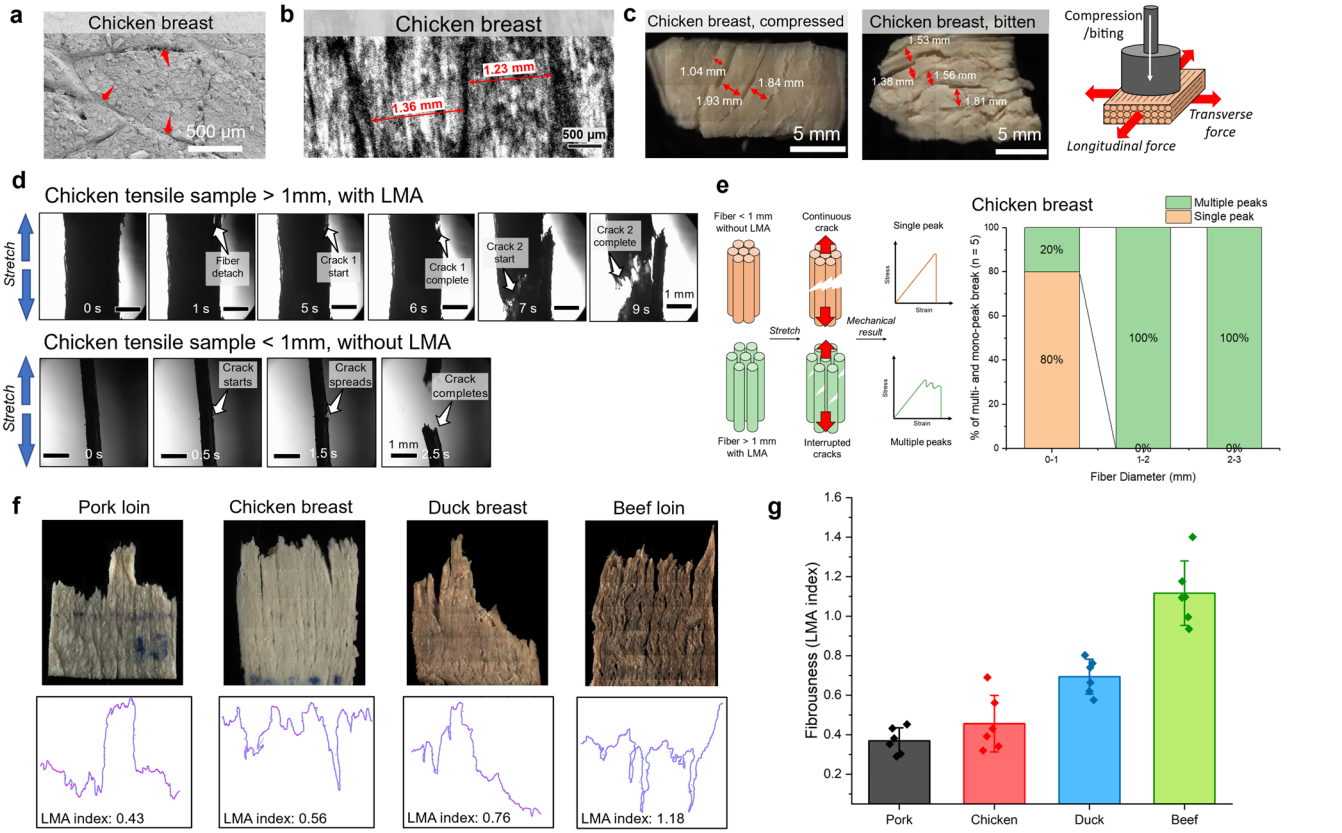

Fig. 1 | Long-range mechanical anisotropy (LMA) provides a measure of fibrousness of animal meat cuts. a SEM images of cross section of boiled meat cuts (pork loin & duck breast in Fig. S1a). Red arrows mark the major gaps located at boundaries between muscle fascicles. **b** OCT from top view of boiled meat cuts (pork loin & duck breast in Fig. S1b). Red arrows mark the size of fascicles with wide gaps at their boundaries. **c** Brightfield imaging of cooked meat cuts after a 75%-strain compression or after being bitten twice by molars (pork loin & duck breast in Fig. S1c), and the illustration of mechanical anisotropy leading to separation of fibers transversely under compression/biting. Red arrows/dashes mark the size of the long fibers with major separation, characterized by the wide longitudinal gaps. **d** Screenshot from high-speed camera videos tearing cooked meat tensile samples with size larger or smaller than muscle fascicles (pork loin & duck breast in Fig. S1d). White arrows and legends mark the development of tensile cracks. **e** Percentage of multi-peak breakage to single-peak breakage on stress-strain curve of cooked meat tensile samples with various sizes in a tensile test ($n = 5$, pork loin & duck breast in Fig. S1e). **f, g** Quantification of fibrousness for different types of meat by the unevenness of their torn edges in an one-dimensional pulling test. The illustration of torn edges extraction and corresponding LMA index (**f**), and the LMA index of different types of meat (**g**).

ellipse best fitting the compressed samples[27]. The aspect ratio of fitting ellipse for HMMA was significantly lower than that of animal meat cuts (Fig. 2f, g, $p < 0.05$). Despite its promising mechanical properties, HMMA's layered structure lacks LMA, preventing it from separating into meat cut-like long fibers with millimeter diameter.

Perforated micro-imprinting confers meat-like LMA and fiber separation of HMMA

To generate meat cut-like fibrousness in HMMA, we developed an imprinting technology to create perforated patterns on sliced HMMA sheets, simulating the gaps between fascicles in animal meats. We sliced HMMA sheets of 1 mm thickness, comparable to muscle fascicles, and imprinted them with a stamp presenting a two-dimensional array of cutting prongs to create perforated patterns (Fig. 3a). These perforations separate the unimprinted areas during consumption, simulating the inter-fascicle separation in animal meats.

Imprinted sheets exhibited meat-like torn edges and separated fibers, reflected by their LMA index comparable to animal meats (Fig. 3b). LMA of imprinted sheets was affected by the imprinting patterns with 4 independent parameters (Fig. 3c): prong length (L), prong width (W), end-to-end prong spacing (S_r), and lateral prong spacing (S_c). S_c was the lateral spacing between adjacent perforated stitches, which directly determined the size of fibers in the imprinted sheets. S_c was thus set at 1 mm to simulate the scale of muscle fascicles (Fig. S3a). The impacts of other three parameters L, W, and S_r on the LMA index were systematically studied by a crossed experimental design (Fig. S3b), with L showing a statistically significant impact that LMA index increased monotonically with higher L values (Fig. S3c). Based on the effect of L on LMA index, we precisely controlled LMA index of imprinted sheets to replicate meat from different species. By varying L from 1.5 mm to 15 mm and fixing S_c, W and S_r at their optimal levels of 1 mm, 0.5 mm and 1 mm respectively, the LMA index increased linearly with increasing L values and covered the range of different types of meat (Fig. 3d). The average LMA indices of imprinted sheets with L values of 4.69 mm, 6.11 mm, 9.32 mm, and 15.29 mm matched those of the tested meat cuts pork loin, chicken breast, duck breast, and beef loin respectively, improving the LMA indices by 1.9 ×, 2.3 ×, 3.5 ×, and 5.6 × higher than the original HMMA (Fig. 3d). The result also suggested that an average L of approximately 5 mm or longer generated LMA comparable to the tested meat cuts. This finding was validated by subjecting imprinted sheets to tensile tests, where the sheets imprinted with L longer than 5 mm showed meat-like multiple peaks on the strain-stress curve (Fig. 3e). The tearing process comparison between imprinted and unimprinted HMMA can be found in the Supplementary Video. The apparent gap between 3 mm and 5 mm might attribute a threshold effect on mechanical measurement related to the stitch length, where the increase from 3 mm to 5 mm significantly created separable fibers detected by tensile peak numbers. Meanwhile, the discrete measurement of peak numbers might be another factor exaggerating the difference between 3 mm and 5 mm. Fixing S_c at the scale of muscle fascicles, higher L values

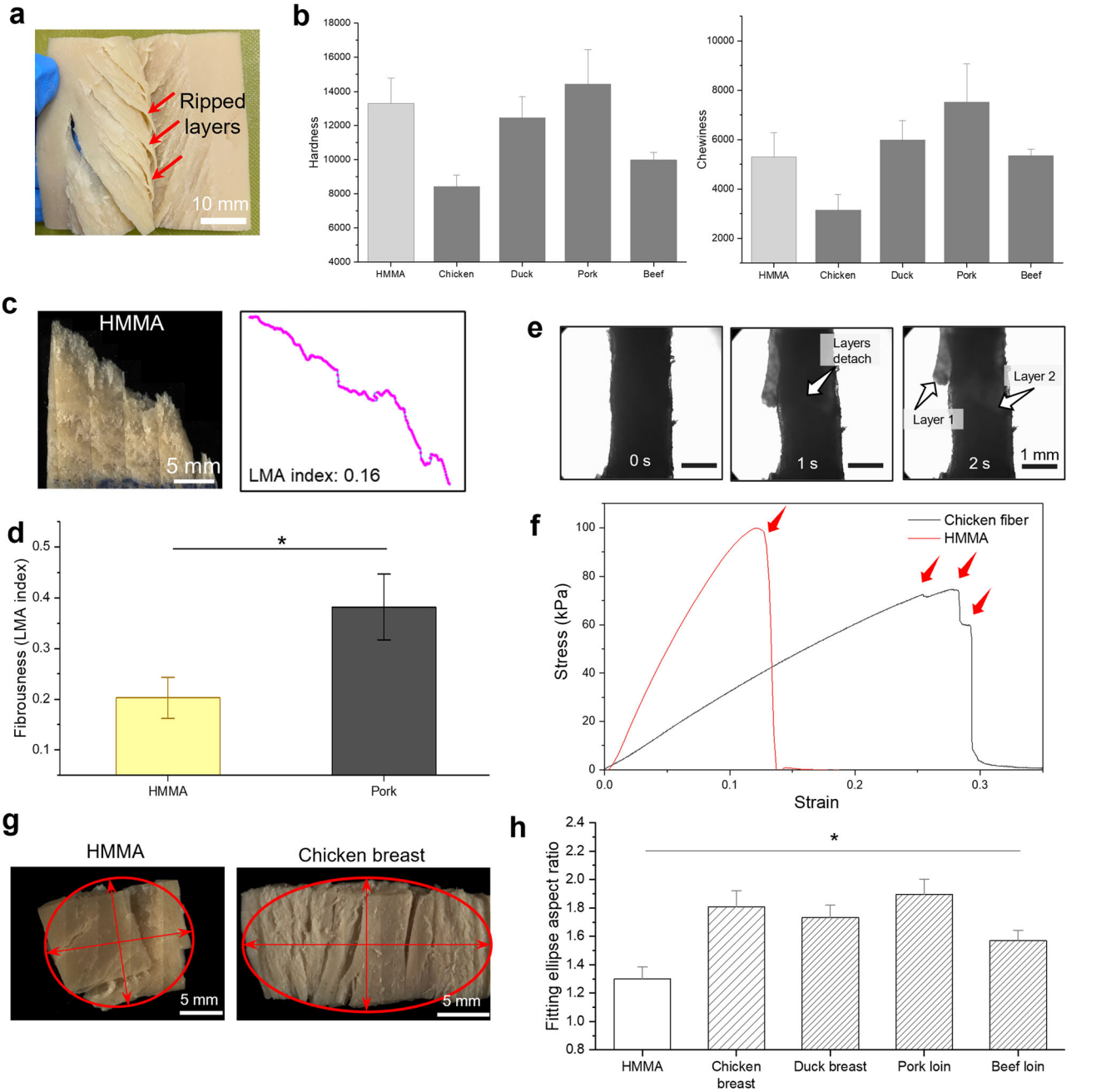

Fig. 2 | HMMA has insufficient LMA to fully replicate meat cut-like fibrousness. **a** The fibrousness of HMMA present by ripping of its layered structure. **b** TPA results of HMMA and different types of meat ($n = 5$, springiness and cohesiveness in Fig. S2). **c** LMA analysis of HMMA and LMA index comparison between HMMA and pork loin ($n = 5$, t-test $^*p < 0.05$). **d** Screenshot from high-speed camera videos tearing HMMA with thickness and width 1–2 mm. White arrows mark the tensile breakdown of HMMA by layer detachment and the resulting two layers. **e** Tensile stress-strain curves of thick tensile samples (diameter 1–2 mm) from HMMA and chicken breast. Red arrows mark the tensile breaking peaks. **f** Brightfield imaging of HMMA and boiled chicken breast cuts after 75%-strain compression. Fitting ellipses with major and minor axis are marked on the images. **g** Representative images of HMMA and animal meat after compression. Fitting ellipses of the compressed samples are shown in red on the images, with major and minor axes marked. **h** Aspect ratio of fitting ellipses of compressed HMMA and different types of meat ($n = 5$, t-test $^*p < 0.05$).

strengthened LMA by increasing the separation between unimprinted areas, resulting in imprinted sheets with meat-like fibrousness that may further construct into imprinted cuts with meat cut-like appearance and mechanical properties.

Imprinted cuts were constructed by binding the imprinted sheets with a commonly used edible binder transglutaminase (TG) that catalyzes the formation of covalent bonds between lysine and glutamine[28,29]. We tested the binding effectiveness of TG powder and TG slurry of different concentrations (Fig. 4a). The effectiveness was evaluated by a shearing test adapted from settings of lap shear strength measurement[30]: a pair of partially bound sheets were clamped at their ends and stretched (Fig. 4b). If the sheets tore without slipping apart, the binding strength was considered sufficient. Otherwise, if they slipped apart before breaking, the binding was insufficient (Fig. 4c). We measured the percentage of effective binding within 6 pairs of each condition, including TG slurry concentrations from 1 wt. % to 10 wt. % and TG powder (TG powder density 1.7 mg/cm^2, comparable to the effective TG density of 10 wt. % TG slurry). It turned out that TG powder and TG slurry concentrations higher than

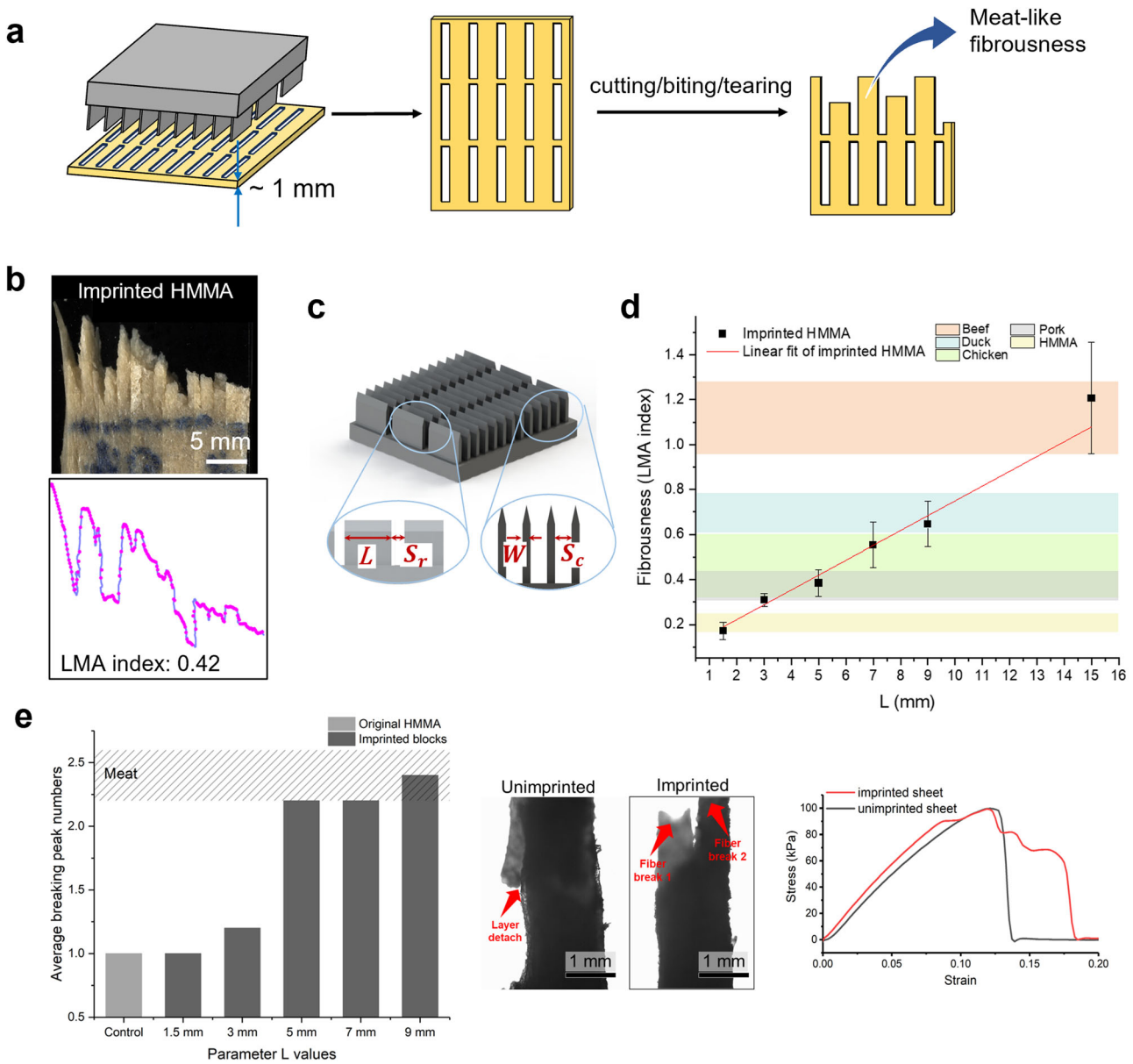

Fig. 3 | Perforated micro-imprinting confers meat-like LMA and fiber separation of HMMA. a Illustration of imprinting HMMA sheets by a stamp and the generation of separable fibers following the perforated imprinting pattern. **b** LMA analysis of an imprinted sheet and its corresponding LMA index. **c** Imprinting stamp design and parameters determining the imprinting pattern. Crossed experimental design results are presented in Fig. S3a-c. **d** Relation between fibrousness (LMA index) and the L values in the imprinted sheets ($n = 5$). Colored regions mark the range (mean ± SD) of LMA index of animal meats and HMMA. **e** Average number of breaking peaks on the stress-strain curve for HMMA sheets without imprinting and imprinted with different patterns ($n = 5$). Meat under the same measurement is shown with slashed lines. Tearing behavior of unimprinted and imprinted sheets under high-speed camera is shown in the middle, and typical curve for multi-peak/single-peak breakage is shown right side.

5 wt. % stably bound imprinted sheets with 100% effectiveness (Fig. 4d). The imprinted cuts constructed by TG slurry or TG powder exhibited texture profiles comparable to animal meats. The hardness, cohesiveness and chewiness of imprinted cuts increased with higher TG slurry concentrations or TG powder (Figs. 4e and S4). Such binding-dependent texture profiles likely result from the tighter binding between the sheets when using higher concentrations TG slurry or TG powder. The springiness of imprinted cuts did not vary by different binding conditions and was close to the original HMMA, suggesting that base material may also affect the properties of imprinted cuts (Fig. 4e). The imprinted cuts with meat-like texture profiles also exhibited meat-like fiber separation at millimeter scale upon compression, characterized by the long fibers separated at millimeter scale (Fig. 4f). The fitting ellipse of compressed imprinted cuts with L longer than 5 mm showed significantly higher aspect ratio than HMMA ($p < 0.05$, Fig. 4f).

Efficient imprinting pattern design for LMA replicating different meats using a machine learning model

Imprinted cuts with LMA separated long and thick fibers upon compression, indicating their meat cut-like fibrousness. Since different types of meat cuts may possess different levels of LMA, their fibrousness can vary accordingly. A rapid and high-throughput imprinting pattern design for different meats' LMA would correlate with different types of meat. We trained a machine learning model, named MLCNet (Meat LMA Carving Network), to correlate imprinting pattern parameters with the compression-induced fiber separation of various imprinted cuts, then

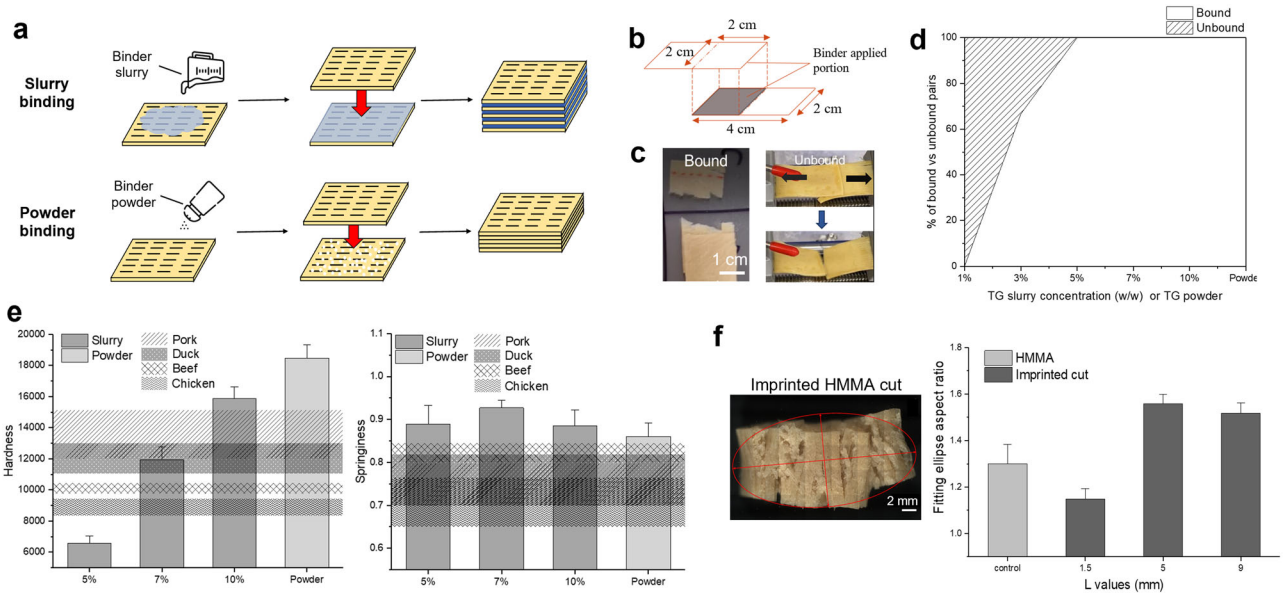

Fig. 4 | Binding imprinted sheets constructs imprinted cuts with meat-like texture profile and anisotropic breakage. a Illustration of TG slurry and powder binding of imprinted sheets. **b**, **c** evaluation of binding strength by a shearing test of partially bound pairs. If the sheets are broken before slipping (c left), their binding is strong enough. **d** Percentage of effectively bound pairs using TG slurry of different concentrations or TG powder ($n = 6$). **e** Texture profile hardness and springiness of meat (shown as patterned area with mean ± SD) and imprinted cuts ($n = 5$, TG powder and TG slurry were used, with slurry concentrations of 5, 7, 10 wt. %). Cohesiveness and chewiness are presented in Fig. S4. **f** Breaking anisotropy of imprinted cuts after a 75%-strain compression, and aspect ratio comparison between fitting ellipses of HMMA and imprinted cuts with L values of 1.5 mm, 5 mm and 9 mm ($n = 5$, t-test $^*p < 0.05$).

applied it to efficiently design suitable patterns for mimicking the LMA of different types of meat (Fig. 5a). MLCNet was validated by comparing its predicted imprinting patterns to those suggested by the LMA analysis for chicken breast, pork loin, and duck breast in Fig. 3d.

We trained MLCNet using images of a set of imprinted cuts with unique patterns after their fiber separation induced by a destructive 75% -strain compression[31,32], reflecting LMA's effect on fibrousness under mechanical loads. To avoid overfitting due to the limited number of images in the training set, we grouped values in each imprinting parameter to improve training efficiency. L values ranging from 1.5 to 9 mm were divided into three equal-length intervals, each represented by two values within the interval—preferably the interval endpoints or an integer within the interval (Fig. 5b). S_c, determining fiber size, was categorized into four values from thin to thick (Fig. 5b). Although variations in W and S_r did not significantly impact LMA according to the previous crossed experiments, we included a set of values of W and S_r for any noticeable differences (Fig. S5a).

Using a convolutional neural network (CNN) based deep learning model, MLCNet successfully identified the critical features driving fiber separation of imprinted cuts. The model effectively distinguished imprinted cuts with different L and S_c values (Fig. 5c), which shows the macro-averaged AUROC 0.867 and 0.813 respectively, but not those with different W and S_r values (the macro-averaged AUROC are 0.685 and 0.710 respectively) due to minimal differences (Fig. S5b). This aligns with our previous findings in crossed experiments that W and S_r did not significantly affect the LMA index of the imprinted sheets (Fig. S3c).

We then applied MLCNet to design L and S_c, the two critical parameters controlling the LMA of imprinted cuts, for replicating the LMA of chicken breast, duck breast, and pork loin. Meat samples were processed similarly to the imprinted cuts by 75%—strain compression to induce fiber separation. Images of these compressed meat samples were fed to the model, which predicted L and S_c values to replicate the observed fiber separation. The predicted values were calculated by comparing meat images to imprinted cuts from different value groups, followed by summing the products of similarity and the weighted average value of each group (Fig. 5d). The values predicted by MLCNet were validated by comparing its predicted imprinting patterns to those suggested by the LMA analysis for chicken breast, pork loin, and duck breast (Fig. 3d). The L values predicted by MLCNet for chicken breast and pork loin closely matched with the values suggested by LMA analysis, while duck breast mismatched likely due to the limited training set (Fig. 5e). Similarly, the model predicted S_c values of approximately 1 mm, matching the observed scale of muscle fascicles (Fig. 5f). Despite the limited training set, MLCNet provided promising results for efficiently designing imprinting patterns for LMA of various animal meats.

Scalable engineering of LMA by continuous imprinting for whole-cut PBM with meat-like sensory profiles

Given the potential of efficient and high-throughput pattern design by MLCNet, an efficient imprinting process is needed for high-volume manufacturing. We designed and built a bench-top continuous imprinting machine to demonstrate efficiency and scalability of LMA control by imprinting. This machine used a roller for continuous imprinting, which improved the overall imprinting speed compared to stepwise stamping (Fig. 6a). Protein sheets placed on a transporting plate were imprinted as the roller rotated through them. Sheets imprinted in this way exhibited fibrousness comparable to the stamped sheets without statistically significant differences in their LMA indices or breaking peak numbers by tensile tests (Fig. 6b, c). This machine prototype demonstrated the feasibility of producing imprinted sheets with meat-like LMA efficiently by a continuous process, making it promising to scale up for a high-volume production.

The sensory properties of imprinted cuts were studied through a biting test and sensory evaluation. Imprinted cuts were bitten twice and then spit out to characterize the structural breakdown during early mastication. Images of the bitten samples were compared with original HMMA controls and animal meat cuts. Imprinted cuts showed meat-like patterns with separated fibers after biting, while original HMMA cuts did not. Differences in structural breakdown patterns were reflected on the PCA plot of the image features extracted by the Local Binary Pattern (LBP) approach[33], with imprinted cuts exhibiting a smaller Euclidean distance of 0.057 to animal meat cuts compared to the 0.106 distance between HMMA and animal meat cuts (Fig. 6d).

To demonstrate the sensory improvement of imprinted cuts, a flamed chicken breast analogue dish was developed for sensory evaluation.

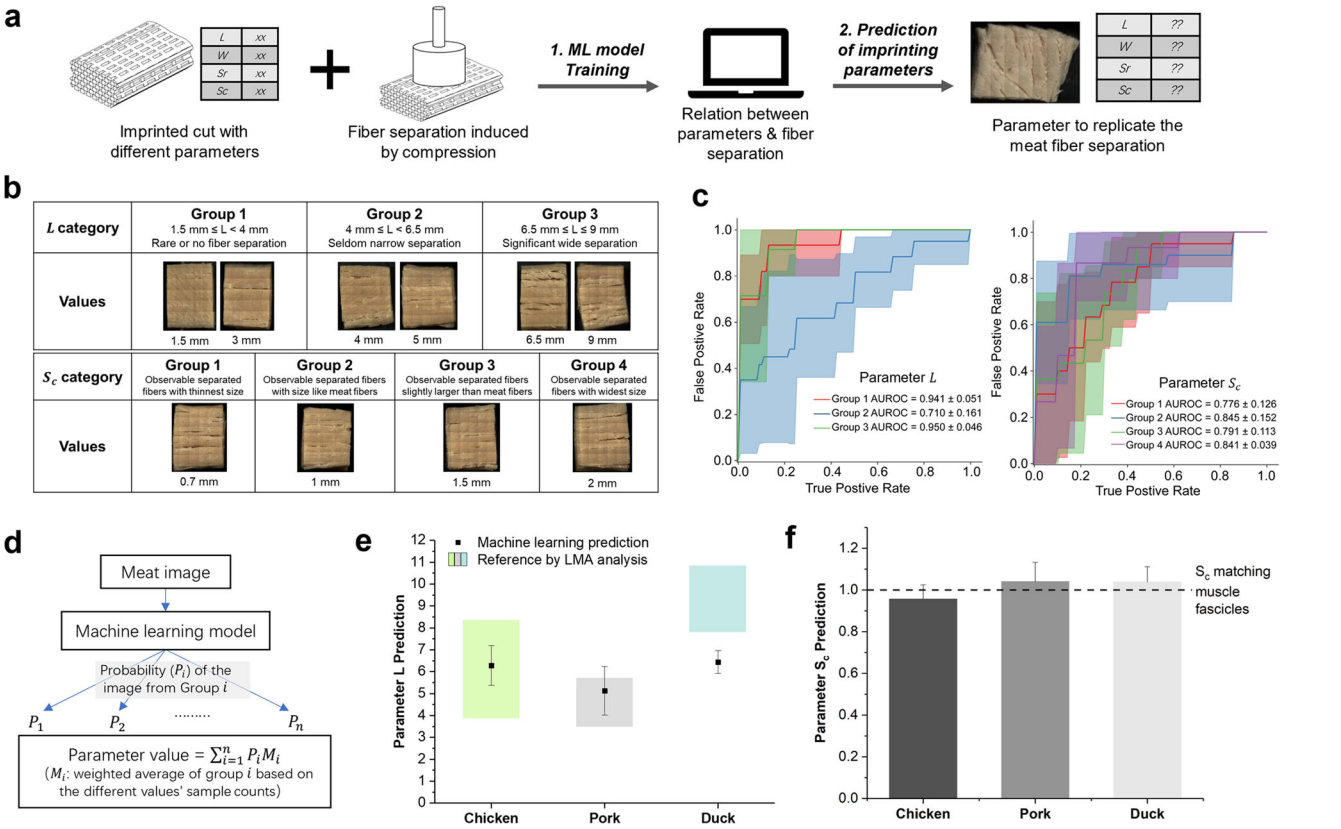

Fig. 5 | Pattern design of imprinted cuts for LMA replicating different meats by a machine learning model. a Illustration of 1. training of the machine learning model to correlate the pattern of separated fibers with imprinting parameters; 2. Application of the model to predict suitable imprinting parameters for the fibrous pattern of specific type of meat. **b** Categorization and representative images in each category of L and S_c values according to their characteristic fibrous patterns. W and S_r category in Fig. S5a. **c** ROC curve of L and S_c groups, both exhibited the recognition of difference between groups (ROC curve of W and S_r in Fig. S5b). **d** Illustration of the process to obtain a suggested imprinting parameter value for certain meat samples. **e** Comparison between the model-predicted L values to replicate animal meat cuts (chicken breast, pork loin, duck breast; black dots, $n = 8$) and the L values calculated from previous LMA analysis (colored regions). **f** S_c to replicate different kinds of meat suggested by the model ($n = 8$). The dashed line shows the proper value to replicate the size of muscle fascicles.

Imprinted cuts were boiled first, followed by marinating in seasonings, and flaming with a torch gun to produce a roasted taste. HMMA and chicken breast controls were prepared similarly to minimize flavor/taste interference. The imprinted cuts exhibited chicken-like appearance with separated fibers, while the original HMMA did not show such fibrousness (Fig. 6e). 15 participants who frequently eat meats evaluated the samples based on overall eating experience and sensory perception of fibrousness. Before presenting participants with the chicken breasts, they were asked to evaluate the satisfaction of overall eating experience focusing on the texture and mouthfeel of imprinted cuts and original HMMA. Compared to original HMMA, imprinted cuts significantly improved overall satisfactions (Fisher's Exact Test, $p < 0.05$, Fig. 6f), showing the capability of imprinting to improve the general eating experience of HMMA. To specifically compare the fibrousness of the two types of analogues, participants were given a piece of real chicken to establish the impression of meat fibrousness before presenting the plant-based analogues. The imprinted samples significantly improved the meat similarity compared to original HMMA in both fibrous appearance and fibrous mouthfeel (Fisher's Exact Test, $p < 0.05$, Fig. 6g). The chicken sample was not provided when evaluating general eating experience because the meaty taste/aroma might interfere participants' judgement on texture and mouthfeel. The participants as meat eaters evaluated the general satisfaction based on their past meat-eating experiences. However, because fibrousness might be an unfamiliar aspect to some participants, chicken breast was provided to establish a standard. Such settings tended to minimize the interference from aroma/taste while keeping a clear comparing standard for participants. To evaluate the potential effect of binding on sensory responses, we performed another sensory evaluation to compare imprinted cuts and unimprinted cuts. Unimprinted cuts were constructed by binding the sliced HMMA sheets without imprinting them. It turned out that imprinted cuts significantly improved consumers' preference when compared to original HMMA, whereas unimprinted cuts did not show significant improvement (Fig. S6).

The results above suggested that conferring meat-like LMA through imprinting simulated meat fibrous appearance and mouthfeel, and significantly improved consumers' general eating satisfaction compared to original HMMA.

Discussion

Animal meat cut is composed of a hierarchical fibrous structure, ranging from myofibrils (approximately 10^0 micrometers in diameter) to muscle fibers (10^1–10^2 micrometers) and muscle fascicles (10^3–10^4 micrometers)[34]. Structures at different scales may not equally influence sensory profiles during meat consumption, and precisely tailoring structures at microscale, such as with 3D printing, can be time- and resource-consuming[35,36]. Therefore, defining the critical scale to replicate meat cut fibrousness is essential for efficiently developing meat-like whole-cut PBM.

In cooked animal meat cuts, muscle fascicles detach more readily than the muscle fibers within the fascicles. This is likely because the perimysium, which connects the fascicles, is more thermal-sensitive than the endomysium connecting muscle fibers[13,18]. Thermal degradation of perimysium results in LMA at muscle fascicle scale, which separates the fascicles to form the long fibers at millimeter scale during meat cut consumption, i.e. the fibrousness of animal meat cuts (Fig. 1).

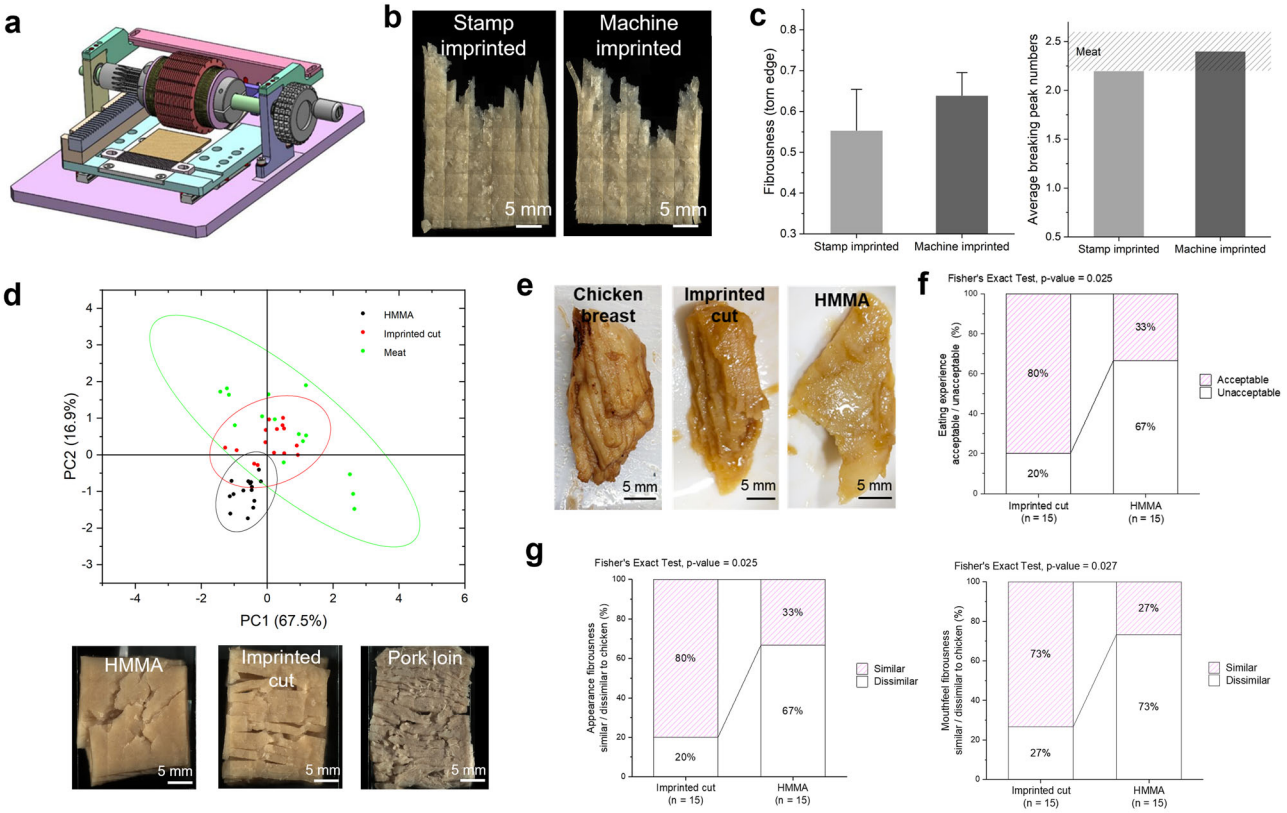

Fig. 6 | Continuous imprinting machine demonstrates the scalable engineering of LMA for whole-cut PBM with meat-like sensory profiles. a Design of a continuous roller-based bench-top imprinting machine. **b** Comparison of the torn sheets imprinted by stamp and machine, where no obvious difference was observed. **c** Comparison between machine-imprinted sheets and stamp-imprinted sheets on their LMA index and the peak numbers on the tensile curve ($n = 5$; 7 mm stamp imprinting was used, stamp imprinting and meat used the same data as Fig. 3d, e for comparison). **d** PCA plot of LBP features extracted from different cuts after biting (HMMA, imprinted cuts; animal meat cut images from chicken breast, duck breast and pork loin). Circled lines show the 95% Confidence Ellipse for each group. Representative images of each type are shown below. **e** Photos of flamed chicken breast dish using conventional chicken breast, imprinted HMMA blocks, and original HMMA. **f** Sensory evaluation results with 15 participants on general eating experience and fibrous similarity to meat. Participants scored the general experience from 1 to 5, indicating very unsatisfying to very satisfying. The analogues with score equal to or higher than 4 were considered having an acceptable eating experience. **g** Participants evaluated the fibrousness in appearance and mouthfeel from 1 to 10, indicating completely different from chicken breast to the same as chicken breast. Scores above and equal to 8 were considered as similar to real chicken. Fisher's Exact Test was applied to analyze the significance of the sensory results, p-value is marked on each graph.

To replicate properties of whole-cut meat, HMMA is widely known for its meat-like mechanical profiles measured by TPA, but it cannot fully replicate meat cut-like fibrousness due to its insufficient LMA (Fig. 2). Various methods have attempted to enhance the fibrousness of HMMA, such as air foaming and inserting micro-composites[37–40]. These methods, although not specifically targeting LMA, slightly enhanced LMA by introducing stress concentrations through air bubbles or composites, resulting in partially improved fibrousness[37,40]. By clearly defining and properly controlling LMA, more significant improvements could be achieved. Recognizing the critical importance of LMA at the fascicle scale, we developed perforated micro-imprinting to precisely control LMA in HMMA. The resulting imprinted cuts significantly improved meat-cut like fibrousness compared to the original HMMA (Figs. 3 and 4).

Imprinting controls LMA by different pattern parameters. Pattern parameter L (prong length) and S_c (lateral prong spacing) were crucial for controlling LMA in the current pattern design (Figs. 3d and 5c). More complex patterns could potentially enhance fiber variety to better mimic the complexity of animal meats. It may worth exploring different prong alignments (aligned vs staggered), prong geometries (straight vs curved), etc., but it should also be noticed that more complicated design might lead to increased fabrication difficulties for high-volume production. LMA might also be affected by other factors such as sheet thickness, but here we focused on imprinting plant-protein sheets to create meat-like fibrousness, other conditions including sheet thickness were maintained at a scale relevant to animal meat, e.g. 1 mm thickness comparable to muscle fascicles. A mechanistic study on LMA under different conditions may be worth exploring in future work to completely understand LMA from structural and mechanical perspective in food materials.

In addition to the LMA, another factor affecting the properties of imprinted cuts is the base material. HMMA was chosen for its mechanical properties generally resembling animal meats (Fig. 2b). While HMMA contributes to the bulk mechanical properties of imprinted cuts, it may also limit certain properties, such as the springiness of the cuts (Figs. 4e and S2). Moreover, HMMA acquires its meat-like mechanical properties through an energy-intensive process involving high temperature and high shearing force[41,42]. This process denatures plant proteins by heating to change their molecular conformation from globules to fibrils and aligning the fibrils through high shearing force[43]. Compared to globular molecules, fibrillar molecules possess improved mechanical properties by exposing more active groups to enhance intermolecular connections[21]. High moisture extrusion processed proteins at molecular scale, which is different from the imprinting that controls fibrousness at millimeter scale relevant to meat fibers. The macroscopic structures of HMMA were changed by imprinting from layers to meat-like fibers, but the molecular structure of HMMA was maintained for mechanical properties. To acquire meat-like mechanical properties, fibrillar plant proteins may not necessarily depend on extrusion as an

energy-intensive process. Methods like producing plant protein amyloid fibrils by acidic pH and mild heating have been developed to improve their mechanical properties[44,45]. Without changing the molecular conformation, other approaches such as optimizing pH, moisture, and ion strength, may also enhance the mechanical properties of plant-protein gels at low energy consumption[46,47]. As an energy-effective process, we foresee the potential of imprinting to create meat-like fibrousness at millimeter scale to enhance the appearance and mouthfeel of plant-protein bases other than HMMA.

We adopted tensile tests to quantify the fibrousness of meat and analogues because of their higher sensitive to micro-structures compared to compression and shearing tests[48]. While tensile tests effectively measure the micro-scale properties of meat fibers, they also allow for the evaluation of some macroscopic properties, such as stiffness, which have been correlated with TPA results[48]. However, because tensile testing is less representative of the human mastication process and there is not a standardized condition that correlates with human mastication[48,49], caution is required when interpreting these measurements to ensure their relevance to human perception. To verify our findings by tensile tests and ensure that our quantitative control of LMA enhanced human sensory satisfaction of meat analogues, we employed other tests including compression, biting, and sensory evaluations from both appearance and mechanical perspectives. Further mechanistic studies on correlation between tensile conditions and human sensory may help improve the interpretation of food measurements by tensile tests.

To evaluate the potential of imprinting in high-volume production, we developed the MLCNet machine learning model to automate pattern design (Fig. 5) and built a roller-based imprinting machine for continuous processing (Fig. 6). AI has been applied in food recognition, quality evaluation, fraud detection, which has demonstrated improvements in the throughput, accuracy, and robustness of food evaluation when supported by large datasets and fraud detection[50–52]. An improved AI model to predict optimal imprinting patterns for whole-cut PBM can be developed with a larger training set and advanced algorithms. While the current MLCNet was tested using meat from different species as example, we foresee the potential of larger AI model applying to mimic meat of different states and qualities with high complexity, e.g. different species, cuts of animals, processing and cooking methods etc. The AI model may achieve automatic and high-throughput pattern selection for imprinting rollers in high-volume production of specific states of meat. Continuous imprinting was demonstrated to be feasible by the roller, and it should be achievable to continuously coat and spread the slurry/powdery binder on imprinted sheets by an on-line liquid sprayer or powder dispenser[53]. The potentially continuous production of imprinted cuts should allow it to fit with high-volume production.

Sensory evaluation is an effective measurement for food that is ultimately judged by human perception. However, when performing sensory evaluation, we also noted some limitations that might be possibly improved in the future. The first issue was the subjective and inconsistent definition of fibrousness among participants. Sensory fibrousness is subjective to participants, and they may have different definitions of fibrous levels. The subjectiveness and inconsistency might result in larger variation when scoring fibrousness. We have attempted to mitigate this issue by providing chicken breast samples to establish the standard of meat fibrousness. Possible improvements may include by training the panelists with a series of standard samples of different defined fibrousness, though established the standard meat samples with different fibrousness might be challenging. The second issue was that strong meaty smell/aroma might distract participants and diminish their sensitivity to texture/mouthfeel. This might be resolved by pinching the noses of participants to reduce their sensitivity to meaty aroma, but pinching nose might change their eating habit and limit their ability to judge food texture as well. It might require recruiting and training panelists specially on meat texture evaluation with pinched nose.

In summary, we identified LMA as a critical structural property to induce the characteristic separation of long fibers in animal meat cuts during consumption. We developed a perforated micro-imprinting technology on HMMA to confer it LMA and meat cut-like fibrousness. Imprinting significantly improved the fibrousness of HMMA according to quantitative measurements and sensory satisfaction. Independent of energy-intensive processing, we foresee imprinting as a scalable and energy-efficient way to produce whole-cut PBM with meat cut-like fibrousness.

Methods

Materials

HMMA was produced from KH Roberts, Singapore. Transglutaminase TG-BP-MH was provided by Ajinomoto, Singapore. Imprinting stamps were 3D printed using formlabs Clear Resin FLGPCL04 at NUS Centre for Additive Manufacturing, Singapore. Raw meats were purchased from a local supermarket. Seasonings used for the prototype dish were purchased at local grocery store.

Cooked meat samples were prepared by method adapted from Christensen et al. with a slight modification[54]. The cooked meat blocks were prepared in this way unless stated separately. The raw meats were defrosted in water bath at room temperature for 30 min, then cut into blocks of around 10 cm × 5 cm × 5 cm. The blocks were then wrapped in aluminum film and sealed in a Ziploc bag before putting into a boiling water bath to heat for 15 min. After boiling for 15 min, the Ziploc bag was put in ice water bath for 5 min to stop cooking. The samples were then taken out and further processed as required for different tests.

High moisture extrusion

High moisture extrusion was performed at KH Robets, Singapore, using extruder ZSE 27 MAXX from Leistritz SEA Pte. Ltd. Soy protein concentrate 40 wt. % and water 60 wt. % were extruded together. Temperatures were set as Zone 1: 40 °C, Zone 2: 50 °C, Zone 3: 60 °C, Zone 4: 70 °C, Zone 5: 90 °C, Zone 6: 100 °C, Zone 7-10: 110 °C. The cooling die was set as TC1: 80 °C, TC2: 60 °C, TC3: 40 °C. Other parameters were not disclosed.

Slicing and imprinting of HMMA sheets

HMMA was produced in bars with thickness around 10 mm. To match the size of separated fiber bundles in conventional meat, and for imprinting to perorate the sheets, the extruded bars were sliced using a meat slicer into sheets of thickness around 1 mm. The sliced sheets were imprinted by 3D printed stamps. The stamps were designed with prongs long enough to imprint through the sheets, and the tip of the prongs were designed sharp to penetrate and perforate the sheets.

Pressing force for the stamp to perforate the sheets was around 75 N on a 2 cm × 2 cm stamp, which was controlled by weights on the stamp. Manual pressing can also generate enough force to perforate the sheets. In this study, manual pressing was used in samples for sensory test and training the machine learning model, to fulfill the demand for large quantity. In other cases, weight-controlling pressing was used.

Transglutaminase (TG) slurry preparation

TG slurry was prepared by mixing TG-BP-MH powder into DI water with different ratios of 1 wt. %, 3 wt. %, 5 wt. %, 7 wt. % and 10 wt. %. The mixture was stirred under room temperature until there was no obvious undissolved clump. The slurry was prepared freshly before binding and use for binding immediately after preparation. For visualization under brightfield microscope, slurry could be mixed with edible dye (0.05 g dye in 10 g slurry, Soft Gel Paste Food Color 218 Burgundy, AmeriColor).

Binding of imprinted HMMA sheets

Imprinted sheets were bound by either TG slurry or directly using TG powder. For slurry binding, around 0.06 g TG slurry was dropped onto the surface of a 2 cm × 2 cm imprinted sheets. Then the slurry was spread across the sheet by a metal scraper to coat the whole surface. For powder binding, around 7 mg TG powders were sprinkled onto imprinted sheets, and it was spread using a metal scraper. After coating binder onto one layer, another layer was put on top of it, with imprinted lines in the same direction. Repeating the above steps several times to get an imprinted stack bound by TG slurry or TG powder. The stack was

then wrapped with cling wrap and kept in a 4 °C fridge overnight to ensure a complete binding.

Binding effectiveness evaluation

Binding effectiveness was evaluated using a setting adapted from lap shear strength measurement[30]. HMMA sheets were sliced and cut into 4 cm × 2 cm sheets, with 1 mm thickness. The sheets were imprinted before coating with binder. The binders, either TG slurry or TG powder, were coated on half of a 4 cm × 2 cm sheet, covering a 2 cm × 2 cm area. Then another 4 cm × 2 cm sheet was put on top of it, with half of the layer overlapping with the binder-coated area. Thus, we combined a pair of sheets with half of each layer overlapping and bound by binders, the other half neither bound nor overlapped at both ends (see in Fig. 4b, c).

The pair of sheets was then clamped on a stretching machine, which clamped the sheets at both ends with single layer, and stretched them in the opposite direction. During the stretching test, if the pair of sheets slipped off from each other without breakage, the binding between them was considered as ineffective. Conversely, if they were torn at either single-layer region or bound region without slipping, the binding was considered as effective. We tested TG powder and a series concentrations of TG slurry including 1 wt. %, 3 wt. %, 5 wt. %, 7 wt. % and 10 wt. %, with 6 pairs in each condition. Number of effectively bound pairs was recorded to evaluate the effectiveness of the binder. We performed pre-test to secure gripping of the sheets, so that there was not sample slipping from the clamps in the 6 pairs during tests.

LMA analysis

Meat samples for LMA analysis were prepared according to the following procedure. Raw meat was initially sliced while frozen using a meat slicer, with the slices cut along the fibers to maintain the majority of fibers parallel to the slicing plane. The resultant raw sheets were approximately 1 mm thick. These sheets were then subjected to cooking in boiling water for 15 seconds, followed by a rapid cooling in an ice water bath for 5 seconds to halt the cooking process. Subsequently, the cooked sheets were sectioned into dimensions of 4 cm × 2 cm, maintaining a thickness of 1 mm. Sheets with excessive fiber cross-sections and insufficient intact fibers were excluded from further testing.

Imprinted HMMA samples for LMA analysis were prepared as follow. HMMA blocks were initially sectioned into sheets measuring 4 cm × 2 cm with a thickness of 1 mm. For imprinting, only the central region of the HMMA sheets, measuring 2 cm × 2 cm, was utilized to ensure uniformity in the thickness of the imprinted area. The imprinting pattern was aligned parallel to the 4-cm side of the sheets.

LMA analysis was conducted as follows: Sheets, whether of cooked meat or imprinted HMMA sheets, were subjected to tensile testing using a stretching machine operating at a constant speed (Fig. S7a). The sheets were secured by clamping 1 cm of material at both ends. Following the tearing process, the sheets were imaged using brightfield microscopy. Sheets that failed to tear cleaning within the clamps were excluded from further analysis. The acquired images were analyzed by MATLAB and ImageJ to delineate the torn edges created during stretching (Fig. S7b, S7c). The *y-axis coordinates* of the torn edges were recorded and annotated by a series of adjacent but discrete dots. Subsequently, every 50 dots were grouped together, and the average *y-axis* coordinate for each group was calculated (the average height point in Fig. S7d). The difference between the average y-axis coordinates of adjacent groups was then calculated by subtracting the *average* coordinate of the group immediately to the left from the *average coordinate* of the current group. The standard deviation of these differences was used as a metric for fibrousness; a higher standard deviation indicated greater fibrousness.

The rationale of using the standard deviation, rather than directly analyzing the *average y-axis coordinate* difference, is based on the need to distinguish between fibrous and non-fibrous edges. A non-fibrous, slanted edge, which either continuously ascends or descends, may exhibit a large average *y-axis coordinate* difference between adjacent points; however, its standard deviation would be small due to the consistent gradient. In contrast, a fibrous edge would exhibit a higher standard deviation due to the irregular and variable nature of the torn edge.

The decision to group every 50 dots, rather than analyzing individual dot, was made to avoid over-analysis of complex and irregular torn edges. Using every single dot could result in excessive detail that may not accurately represent the overall fibrousness. After evaluating various group sizes, grouping every 50 dots was found to provide a balanced and effective measure (Fig. S8). More details regarding this methodology can be found in the Supplementary Information.

Destructive compression test to simulate structural damage during consumption

To induce structural damage in cooked meat and HMMA samples (imprinted and unimprinted) simulating their consumption, a destructive compression test was conducted, and structural changes were compared before and after compression. The compression was done by a hydraulic presser, which had two parallel metal plates that allow the samples to be compressed between them. Samples were prepared as 1 cm × 1 cm × 1 cm blocks if not specified. Meat samples were cut to expose as many fibers on the top 1 cm × 1 cm surface as possible. Imprinted samples were prepared by stacking and binding the imprinted sheets. The samples were placed between the plates. The samples were then compressed by the plates until 75% strain, which is considered as a destructive strain in uniaxial test[55]. The fiber separation morphology was then captured by brightfield imaging for further analysis.

Image acquisition for machine learning model

Imprinted cuts were prepared using stamps of different patterns, with L of 1.5, 3, 4, 5, 6.5, 9 mm; W of 0.5, 1, 1.5, 2 mm; S_c of 0.7, 1, 1.5, 2 mm; S_r of 1, 2, 3, 4 mm. While varying one parameter, the other three parameters were fixed at one level with L of 6.5 mm, W of 0.5 mm, both S_c and S_r of 1 mm. 2 × 2 × 1 cm blocks were constructed in each pattern following the methods mentioned above using TG powder as binder. Cooked meat samples by chicken breast, duck breast, and pork loin were prepared as mentioned above and cut into blocks of comparable 2 × 2 × 1 cm size.

Fiber separation of imprinted cuts and meat samples was induced by the 75% strain compression using the hydraulic presser. The compressed samples were imaged by brightfield imaging. The images were then used for the machine learning model.

Data pre-processing for machine learning model

All raw images acquired from tissue scanner microscopy were converted into gray-scale for texture feature extractions using standard linear algorithm implemented by OpenCV (Python package). Images then were categorized into different groups based on their respective imprinting parameters. Specifically, we classified L into 3 groups ($1.5 \le L < 4.0$, $4.0 \le L < 6.5$, $6.5 \le L \le 9.0$), which resulting in 27, 19 and 28 images respectively. Similarly, for parameter W, S_c and S_r, we split the data into 4 groups with corresponding image numbers (The distribution of different datasets was W: 0.5:21, 1:17, 1.5:12, 2:12; S_r: 1:21, 2:12, 3:12, 4:12; S_c: 0.7:12, 1:21, 1.5:12, 2:12). The criterion for L categorization is the significance of fiber separation from low to high. The criterion for S_c categorization is the size of separated fibers, where the width increased accordingly with higher S_c values. For S_r and W, since no significant difference was observed between different values, each value was directly assigned to be one group to check if the model was able to identify any differences.

Multi-instance learning and deep learning model

After obtaining four independent developing datasets, our objective is to train four different deep learning models for predicting continuous meat parameters by learning knowledge from its visual features. Each model employs the same structure and training strategies. The process begins with a random partition of each individual dataset into training and validation sets. Subsequently, we apply a center crop to each image to remove the

background and resize it to a consistent 2240 × 2240-pixel dimension, ensuring uniformity in the number of patches after the split. This approach allowed us to expand our dataset significantly, increasing the number of samples from approximately 100 to over 7000. These 224 × 224-pixel patches are then normalized and input into a pretrained ResNet-18 model for feature extraction. The extracted patch features from each image are concatenated and fed into an attention pooling network with a SoftMax layer for group classification. We utilized the Adam optimizer and trained the model for 100 epochs with a learning rate of 0.0002. During training, only the multi-instance classifier is tunable while we froze the visual feature backbone. For each dataset, we conducted 5-fold cross-validation and selected the model with the best performance for meat prediction during testing. Different from conventional classification metrics including accuracy or confusion matrices to describe the model performance, we calculated the potential parameters for each type of meat by computing the weighted predicted score, which is the sum of the product of the predicted probability of each class and the average parameter value in that group. All the analytical processes were implemented by Python and PyTorch.

Fitting ellipse analysis of destructively compressed samples

Samples were prepared into cubes with comparable sizes of 1 × 1 × 1 cm, with the fibrous surface facing top. The cubes were then compressed by a hydraulic presser with 75% strain to induce destructive structural changes. After being compressed, the samples were imaged under a tissue scanner microscope. The captured images were converted to binary using ImageJ, and the fitting ellipse of the binarized image was obtained by ImageJ. Aspect ratio of the fitting ellipses was obtained by the ratio of major axis length to the minor axis length.

Brightfield imaging

Brightfield images were taken using tissue scanner microscopy by TissueGnostics TissueFAXS Plus at 2.5 ×. An external light source was added to allow reflective light imaging.

Scanning electronic microscopy (SEM)

Meat samples for SEM viewing were fixed in 2.5% glutaraldehyde overnight in 4 °C. The samples were then washed in PBS 2 times and osmicated with 1% Osmium Tetraoxide (OsO_4) for 2 h, followed by washing with distilled water for 2 times with 10 min each time. Subsequently, the samples were subjected to ethanol series for dehydration: 25% ethanol for 5 min, 50% ethanol for 10 min, 75% ethanol for 10 min, 95% ethanol for 10 min, and 100% ethanol 3 times with 10 min each time. Afterwords, the samples were dried using critical point dryer LEICA CPD300, and then sticked onto a sample plate with double sided carbon tape. The samples were gold coated using LEICA ACE200. Viewing was performed by Thermofisher FEI Quanta 650 FEG-SEM.

Optical coherence tomography (OCT)

Meat samples for OCT were cooked in the way as described above, and subsequently cut into blocks of 2 cm × 2 cm × 1 cm, with as many fibers exposed on the 2 cm × 2 cm surface as possible. The cooked meat blocks were scanned under OCT (OptoRes, 1300 nm NG-FDML), with 2 cm × 2 cm surface facing the OCT camera on the top. Scanned images were processed using ImageJ to reslice it for top view of the sample's fibrous surface, followed by doing a Z projection with average intensity of the slices. The distances were measured between wide gaps with length almost across the image, which were considered as major detachment between the fibers.

Tensile fracture of meat fibers characterized under high-speed camera

Meat samples for high-speed camera were cooked as described above. Afterwards, cooked meat cuts were peeled to isolate meat strips of specific diameters (< 1 mm or > 1 mm). The strips were then clamped on a tensile device, which allowed to tear the strips by stretching in opposite directions, and to view the tearing process under a microscope. The microscope was equipped with a high-speed camera, which allowed us to better capture the difference in breaking behavior between thin strips (< 1 mm) and thick strips (> 1 mm). The stretching process was recorded by video, and the video was further processed to extract the frames where the breakages happened. The complexity was shown by identifying its breakage behavior. High-speed camera and microscope characterizations were performed by inverted microscope (IX71, Olympus, Japan) equipped with a high-speed CCD camera (Phantom v9, Vision Research, USA).

Tensile test by universal testing machine

Mechanical complexity was analyzed by tensile tests of cooked meat fibers with different sizes. The cooked meat fibers were obtained by cooking the meat cuts as described above, followed by peeling the meat strips of different sizes from the cooked blocks. Strip sizes were measured using a caliper, and divided into ranges of < 1 mm, 1–2 mm, and 2–3 mm. The strips were then clamped on the tensile fixture of a universal testing machine (Instron, Model 68SC-2 Single Column Table Model, USA). Tensile test was performed at speed of 20% strain/min to evaluate whether the fibers broke with single peak or multiple peaks on the strain-stress curve. 5 samples were tested in each diameter range, and the number was recorded for fibers with single-peak and multi-peak breakage.

Tensile test for imprinted sheets were performed in a similar way but the sheets were prepared in dumbbell shape adapted from Honikel[56] with a comparable cross section area to the 1 mm think meat fiber bundles. The peak numbers on stress-strain curves were calculated by counting the numbers of zero points for derivatives of the curves.

Texture profile analysis

Texture profile analysis by a two-cycle compression test was performed under room temperature using TA.XTplus Texture Analyzer from Stable Micro Systems. Probe: P/36 R. Testing settings: Pre-Test Speed 1.00 mm/s, Test Speed 1.00 mm/s, Post-Test Speed 5.00 mm/s. Target Mode: Strain, Strain: 50.0%, Time: 3.00 s. Trigger Type: Auto (Force), Tigger Force: 5.0 g. Samples were prepared in shape of 2 cm × 2 cm × 1 cm blocks before test.

Prototype dish preparation

HMMA was sliced and cut to form rectangular HMMA sheets of 4 cm × 6 cm and 1 mm thick. These sheets were imprinted and bound by TG powder to form a stack. Each stack was constructed by 7 layers of imprinted sheets. Original HMMA bars were used as control, which were also cut into 4 cm × 6 cm blocks, with comparable thickness to the imprinted stacks. Both imprinted stacks and original HMMA blocks were torn randomly into pieces to mimic that of chicken strips. Subsequently, the torn pieces were boiled at 100 °C for 2 mins, drained of excess moisture and cooled to room temperature. Following, seasonings and flavorings were added to replicate the taste of smoked chicken strips. The pieces were marinated at room temperature for at least 30 minutes, and flame torched for approximately 45 seconds to further enhance the smoky flavor and create a color of barbequed chicken strips.

Lean chicken breast meat was boiled in hot water till fully cooked and torn into pieces of similar size to the HMMA pieces. Subsequently, the chicken strips were also marinated and flame torches with the exact same procedure as mentioned above.

Consumer acceptability evaluation

Sensory evaluation was carried out among a panel of 15 assessors. Informed consent was obtained from all the participants. In this single-blind test, participants were tasked to evaluate the general eating experience and the fibrous appearance and texture of the cooked imprinted pieces as compared to original HMMA and real chicken pieces. Imprinted pieces and original HMMA samples were coded with a three-digit number and order of samples was randomized. Participants were given the samples sequentially and asked to make choices among options regarding their general eating experience and the similarity of the samples to chicken breast in terms of their fibrousness in appearance and texture. After being presented with one

sample, participants had to evaluate and grade it based on a series of questions before they were given the next sample. Participants were not allowed to change their evaluation scores of previous samples to eliminate biasness. The participants were asked to evaluate the satisfaction of general eating experience of imprinted cuts and original HMMA without knowing the sample types. As meat eaters, participants evaluated the satisfaction based on their past meat-eating experiences without tasting the real chicken breast samples. The chicken samples were not provided at this step to avoid interference from chicken's meaty smell, taste or aroma. The participants were then informed and given a piece of sample from real chicken breast, then they were given the two types of plant-based meat samples again without knowing the sample types. They were then asked to evaluate the fibrous appearance and mouthfeel of the plant-based meat samples. The chicken samples were provided at this step as fibrousness might not be a property commonly noted in their experiences. The results of general eating experience were transformed to 1–5, 1 meaning very unsatisfying and 5 meaning very satisfying. The results of fibrous similarity to chicken breast were transformed to 1–10. Fisher's Exact Test was performed to examine the significance of difference. In general eating experience, samples with score above and equal to 4 (out of range 1–5) were categorized as acceptable while samples below 4 (out of range 1–5) were categorized as unacceptable for Fisher's Exact Test. In fibrousness comparison, samples with score above and equal to 8 (out of range 1–10) were categorized as similar to chicken while samples below 8 (out of range 1–10) were categorized as unsimilar to chicken for Fisher's Exact Test.

For sensory evaluation comparing unimprinted cuts and imprinted cuts, samples including original HMMA, unimprinted cuts and imprinted cuts were prepared following the same protocol above, with the only difference being that unimprinted cuts were constructed by sliced sheets without imprinting. Eight participants were asked to score their preference of the samples based on their meat-eating experiences. They could score the samples with 1, 2 or 3 with 1 meaning the least preferred and 3 meaning the most preferred. Each sample should be marked with one number while no numbers could be used twice. Fisher's Exact Test was used to evaluate the significance, where score 1 with lowest preference was categorized as unacceptable to consumers, 2 or 3 with medium to high preference were categorized as acceptable. All the participants were meat eaters.

Statistical analysis

Crossed design for pattern parameters of different values was performed by Minitab using Taguchi design, and the results were analyzed using the same software to get the main effect plot and pareto chart of the standardized effect. Fisher's Exact Test was performed using MATLAB. Other statistical analyses including *t*-Test, and linear fitting were performed using OriginPro.

Data availability

The data that support the findings of this study are available from the corresponding author, Hanry Yu (phsyuh@nus.edu.sg) upon reasonable request.

Code availability

The code used in this study is available from the corresponding author, Hanry Yu (phsyuh@nus.edu.sg) upon reasonable request.

Received: 1 July 2024; Accepted: 14 November 2024;
Published online: 20 December 2024

References

1. Kumar, P. et al. In-vitro meat: a promising solution for sustainability of meat sector. *J. Anim. Sci. Technol.* **63**, 693–724 (2021).
2. Gerber, P. J. et al. *Tackling climate change through livestock: a global assessment of emissions and mitigation opportunities*. (Food and Agriculture Organization of the United Nations (FAO), 2013).
3. Font, I. F. M. Meat Consumption, Sustainability and Alternatives: An Overview of Motives and Barriers. *Foods* **12**, https://doi.org/10.3390/foods12112144 (2023).
4. Santo, R. E. et al. Considering Plant-Based Meat Substitutes and Cell-Based Meats: A Public Health and Food Systems Perspective. *Front. Sustain. Food Syst.* **4**, https://doi.org/10.3389/fsufs.2020.00134 (2020).
5. Wang, Y. et al. The development process of plant-based meat alternatives: Raw material formulations and processing strategies. *Food Res Int* **167**, 112689 (2023).
6. Wang, Y., Cai, W., Li, L., Gao, Y. & Lai, K. H. Recent Advances in the Processing and Manufacturing of Plant-Based Meat. *J. Agric Food Chem.* **71**, 1276–1290 (2023).
7. Yang, L., Zhang, T., Li, H., Chen, T. & Liu, X. Control of Beany Flavor from Soybean Protein Raw Material in Plant-Based Meat Analog Processing. *Foods* **12**, https://doi.org/10.3390/foods12050923 (2023).
8. McClements, D. J. & Grossmann, L. Next-Generation Plant-Based Foods: Challenges and Opportunities. *Annu Rev Food Sci Technol*, https://doi.org/10.1146/annurev-food-072023-034414 (2023).
9. Dekkers, B. L., Boom, R. M. & van der Goot, A. J. Structuring processes for meat analogues. *Trends Food Sci. Technol.* **81**, 25–36 (2018).
10. Zohdi, N. & Yang, R. C. Material Anisotropy in Additively Manufactured Polymers and Polymer Composites: A Review. *Polymers (Basel)* **13**, https://doi.org/10.3390/polym13193368 (2021).
11. Chang, H. et al. Effect of Heat-Induced Changes of Connective Tissue and Collagen on Meat Texture Properties of BeefSemitendinosusMuscle. *Int. J. Food Prop.* **14**, 381–396 (2011).
12. Astruc, T., Gatellier, P., Labas, R., Lhoutellier, V. S. & Marinova, P. Microstructural changes in m. rectus abdominis bovine muscle after heating. *Meat Sci.* **85**, 743–751 (2010).
13. Zheng, Y. Y. et al. Evaluating the effect of cooking temperature and time on collagen characteristics and the texture of hog maw. *J. Texture Stud.* **52**, 207–218 (2021).
14. Ilic, J., Djekic, I., Tomasevic, I., Oosterlinck, F. & van den Berg, M. A. Materials Properties, Oral Processing, and Sensory Analysis of Eating Meat and Meat Analogs. *Annu Rev. Food Sci. Technol.* **13**, 193–215 (2022).
15. Witte, F. et al. Influence of Finely Chopped Meat Addition on Quality Parameters of Minced Meat. *Appl. Sci.* **12**, https://doi.org/10.3390/app122010590 (2022).
16. Berger, L. M., Witte, F., Terjung, N., Weiss, J. & Gibis, M. Influence of Processing Steps on Structural, Functional, and Quality Properties of Beef Hamburgers. *Appl. Sci.* **12**, https://doi.org/10.3390/app12157377 (2022).
17. Lillford, P. J. The materials science of eating and food breakdown. *Mrs Bull.* **25**, 38–43 (2000).
18. Light, N. & Champion, A. E. Characterization of muscle epimysium, perimysium and endomysium collagens. *Biochem. J.* **219**, 1017–1026 (1984).
19. van der Sman, R. G. M. & van der Goot, A. J. Hypotheses concerning structuring of extruded meat analogs. *Curr. Res Food Sci.* **6**, 100510 (2023).
20. Sha, L. & Xiong, Y. L. Plant protein-based alternatives of reconstructed meat: Science, technology, and challenges. *Trends Food Sci. Technol.* **102**, 51–61 (2020).
21. Zhang, Z. et al. High-moisture Extrusion Technology Application in the Processing of Textured Plant Protein Meat Analogues: A Review. *Food Rev. Int.* 1–36, https://doi.org/10.1080/87559129.2021.2024223 (2022).
22. Cornet, S. H. V. et al. Thermo-mechanical processing of plant proteins using shear cell and high-moisture extrusion cooking. *Crit. Rev. Food Sci. Nutr.* **62**, 3264–3280 (2022).

23. Schreuders, F. K. G. et al. Comparing structuring potential of pea and soy protein with gluten for meat analogue preparation. *J. Food Eng.* **261**, 32–39 (2019).
24. Sun, C., Fu, J., Chang, Y., Li, S. & Fang, Y. Structure Design for Improving the Characteristic Attributes of Extruded Plant-Based Meat Analogues. *Food Biophys.* **17**, 137–149 (2021).
25. Oppen, D., Grossmann, L. & Weiss, J. Insights into characterizing and producing anisotropic food structures. *Crit. Rev. Food Sci. Nutr.* **64**, 1158–1176 (2024).
26. Willems, M. E. & Purslow, P. Mechanical and structural characteristics of single muscle fibres and fibre groups from raw and cooked pork longissimus muscle. *Meat Sci.* **46**, 285–301 (1997).
27. Mulchrone, K. F. & Choudhury, K. R. Fitting an ellipse to an arbitrary shape: implications for strain analysis. *J. Struct. Geol.* **26**, 143–153 (2004).
28. Schopfer, L. M., Onder, S. & Lockridge, O. Evaluation of mass spectrometry MS/MS spectra for the presence of isopeptide crosslinked peptides. *PLoS One* **16**, e0254450 (2021).
29. Miwa, N. Innovation in the food industry using microbial transglutaminase: Keys to success and future prospects. *Anal. Biochem* **597**, 113638 (2020).
30. Ferraris, M. et al. Torsion Test vs. Other Methods to Obtain the Shear Strength of Elastic-Plastic Adhesives. *Appl. Sci.* **12**, https://doi.org/10.3390/app12073284 (2022).
31. Rosenthal, A. J. Texture Profile Analysis - How Important Are the Parameters? *J. Texture Stud.* **41**, 672–684 (2010).
32. Lu, R. In *Instrumental assessment of food sensory quality* 103-128 (Elsevier, 2013).
33. Probst, Y., Nguyen, D. T., Tran, M. K. & Li, W. Dietary Assessment on a Mobile Phone Using Image Processing and Pattern Recognition Techniques: Algorithm Design and System Prototyping. *Nutrients* **7**, 6128–6138 (2015).
34. Gotti, C., Sensini, A., Zucchelli, A., Carloni, R. & Focarete, M. L. Hierarchical fibrous structures for muscle-inspired soft-actuators: A review. *Appl. Mater. Today* **20**, https://doi.org/10.1016/j.apmt.2020.100772 (2020).
35. Portanguen, S., Tournayre, P., Sicard, J., Astruc, T. & Mirade, P.-S. In *Future Foods* 627-644 (2022).
36. Dong, H., Wang, P., Yang, Z. & Xu, X. 3D printing based on meat materials: Challenges and opportunities. *Curr. Res Food Sci.* **6**, 100423 (2023).
37. Zink, J. I., Zeneli, L. & Windhab, E. J. Micro-foaming of plant protein based meat analogues for tailored textural properties. *Curr. Res Food Sci.* **7**, 100580 (2023).
38. Ghanghas, N., Nadimi, M., Paliwal, J. & Koksel, F. Gas-assisted high-moisture extrusion of soy-based meat analogues: Impacts of nitrogen pressure and cooling die temperature on density, texture and microstructure. *Innovative Food Sci. Emerg. Technol.* **92**, https://doi.org/10.1016/j.ifset.2023.103557 (2024).
39. Dobson, S., Laredo, T. & Marangoni, A. G. Particle filled protein-starch composites as the basis for plant-based meat analogues. *Curr. Res Food Sci.* **5**, 892–903 (2022).
40. Taghian Dinani, S., Broekema, N. L., Boom, R. & van der Goot, A. J. Investigation potential of hydrocolloids in meat analogue preparation. *Food Hydrocolloids* **135**, https://doi.org/10.1016/j.foodhyd.2022.108199 (2023).
41. Zhang, J., Liu, L., Jiang, Y., Faisal, S. & Wang, Q. A new insight into the high-moisture extrusion process of peanut protein: From the aspect of the orders and amount of energy input. *J. Food Eng.* **264**, https://doi.org/10.1016/j.jfoodeng.2019.07.015 (2020).
42. Liang, M., Huff, H. E. & Hsieh, F. H. Evaluating Energy Consumption and Efficiency of a Twin-Screw Extruder. *J. Food Sci.* **67**, 1803–1807 (2006).
43. Zhang, J., Chen, Q., Kaplan, D. L. & Wang, Q. High-moisture extruded protein fiber formation toward plant-based meat substitutes applications: Science, technology, and prospect. *Trends Food Sci. Technol.* **128**, 202–216 (2022).
44. Li, T. et al. Plant Protein Amyloid Fibrils for Multifunctional Sustainable Materials. *Adv. Sustain. Syst.* **7**, https://doi.org/10.1002/adsu.202200414 (2023).
45. Cao, Y. & Mezzenga, R. Food protein amyloid fibrils: Origin, structure, formation, characterization, applications and health implications. *Adv. Colloid Interface Sci.* **269**, 334–356 (2019).
46. Zhou, H., Hu, X., Xiang, X. & McClements, D. J. Modification of textural attributes of potato protein gels using salts, polysaccharides, and transglutaminase: Development of plant-based foods. *Food Hydrocolloids* **144**, https://doi.org/10.1016/j.foodhyd.2023.108909 (2023).
47. Tan, Y., Zhang, Z. & McClements, D. J. Preparation of plant-based meat analogs using emulsion gels: Lipid-filled RuBisCo protein hydrogels. *Food Res Int* **167**, 112708 (2023).
48. Schreuders, F. K. G., Schlangen, M., Kyriakopoulou, K., Boom, R. M. & van der Goot, A. J. Texture methods for evaluating meat and meat analogue structures: A review. *Food Control* **127**, https://doi.org/10.1016/j.foodcont.2021.108103 (2021).
49. Schlangen, M., Schlangen, E. & van der Goot, A. J. Advanced tensile testing as a new tool to quantify properties of food. *Curr. Res Food Sci.* **7**, 100577 (2023).
50. Othman, S., Mavani, N. R., Hussain, M. A., Rahman, N. A. & Mohd Ali, J. Artificial intelligence-based techniques for adulteration and defect detections in food and agricultural industry: A review. *J. Agric. Food Res.* **12**, https://doi.org/10.1016/j.jafr.2023.100590 (2023).
51. Hategan, A. R. et al. Opportunities and Constraints in Applying Artificial Neural Networks (ANNs) in Food Authentication. Honey—A Case Study. *Appl. Sci.* **11**, https://doi.org/10.3390/app11156723 (2021).
52. Goyal, K., Kumar, P. & Verma, K. Food Adulteration Detection using Artificial Intelligence: A Systematic Review. *Arch. Comput. Methods Eng.* **29**, 397–426 (2021).
53. Lupoi, R. & O'Neill, W. Powder stream characteristics in cold spray nozzles. *Surf. Coat. Technol.* **206**, 1069–1076 (2011).
54. Christensen, M., Purslow, P. P. & Larsen, L. M. The effect of cooking temperature on mechanical properties of whole meat, single muscle fibres and perimysial connective tissue. *Meat Sci.* **55**, 301–307 (2000).
55. Rahman, M. S., Al-Attabi, Z. H., Al-Habsi, N. & Al-Khusaibi, M. Measurement of instrumental texture profile analysis (TPA) of foods. *Techniques to Measure Food Safety and Quality: Microbial, Chemical, and Sensory*, 427–465 (2021).
56. Honikel, K. O. Reference methods for the assessment of physical characteristics of meat. *Meat Sci.* **49**, 447–457 (1998).

Acknowledgements

This work is supported in part by Good Food Institute; Institute of Bioengineering and Bioimaging (IBB), A*STAR; Institute for Digital Medicine (WisDM); NMRC (CIRG21nov-0032); and Mechanobiology Institute of Singapore funding to H.Y. S.N. is supported by Enterprise Singapore T-UP funding through A*STAR for secondment to Ants Innovate.

Author contributions

X.L. and H.Y. conceived the study, designed the experiments, supervised, and organized the coworkers. X.L. developed imprinting and binding process, LMA analysis, drafted the manuscript, and performed major data collection. J.W. trained the machine learning model and generated the model-recommend patterns for different types of meat. L.G.K. prepared samples for machine learning model training, performed TissueFAXS and SEM imaging, developed prototype dish of flamed chicken analogue using imprinted cuts, and designed the sensory evaluation. H.Z. organized the sensory evaluation sessions and processed the sensory evaluation data. F.Y.T.O. processed data from universal testing machine, and prepared

samples for sensory evaluation. S.N. advised on the development of the research and data collection.

Competing interests

The authors declare potential competing interests as S.N. is seconded from A*STAR to work in the spin-off, Ants Innovate and declares no non-financial competing interests; Author H.Y. holds shares in Ants Innovate and declares no non-financial competing interests. All other authors declare no financial or non-financial competing interests.

Ethics approval

The experiments involving human participants were performed following the approval of the National University of Singapore Institutional Review Board (Reference code: NUS-IRB-2024-853).

Additional information

Supplementary information The online version contains supplementary material available at https://doi.org/10.1038/s41538-024-00344-0.

Correspondence and requests for materials should be addressed to Hanry Yu.